ISSN 1392–1207. MECHANIKA. 2022 Volume 28(2): 103–112

Optimization and Control of Vehicle Vertical System with Suspended In-Wheel Motor

Jinwei SUN*, Jingyu CONG**
**School of Vehicle Engineering, Xi'an Aeronautical University, Xi'an 710077, China, E-mail: jinweisunbit@126.com*
***School of Information and Communication Engineering, Hainan University, Haikou 570228, China,*
E-mail: jingyuconghnu@126.com (Corresponding author)
crossref http://dx.doi.org/10.5755/j02.mech.30770

1. Introduction

Due to the growing popularity of electric vehicles (EVs) in modern automotive industry in recent years, significant research has been conducted on the topic [1-3]. From the perspective of driving mode, there are two types of motor configurations used in EVs: centralized motors and distributed drive with in-wheel motors (IWM). Compared with the centralized driven type, the IWM configuration of EVs provides a new research direction for its advantages such as lightweight, space consumption, high performance and energy efficient etc [2]. There is a wide variety of motors available for EVs, including induction motor, synchronous motor and switch reluctance motor (SRM). Although permanent magnet synchronous motors (PMSM) are currently the main form of electric vehicle drive motors [3], the permanent magnet patch strength, rate-earth material costs and demagnetization hindering its further application in EV drive motors. Then the SRM was raised as a strong alternative for future motorized wheels with its simple and reliability structure, large starting torque, wide speed range and flexible control [4].

For the vehicle vertical system, the special configuration of the IWM directly connected to the wheel hub leads to negative vibration effect induced by the increase of unsprung mass [5] and motor unbalance electromagnetic force [6], which will seriously affect the comfort and safety of vehicles. In view of above problems, many new vibration isolate structures different from tradition IWM have been proposed to reduce the undesired vibrations. To reduce the vibration caused by increased unsprung mass, an integrated IWM with elastic sleeve connection was brought out by Wang to minimize the deteriorated vibration of electric wheel [7]. Taking magnetic gap deformation of the propulsion motor arise from road excitation into consideration, Luo and Tan designed a new IWM topology through placing the rubber bushing IWM to flexibly separated the motor mass from the unsprung mass [8]. Apart from flexible material-based vibration isolator, the dynamic vibration absorber with parallel spring and damper have also been utilized to improve the IWM-suspension performance. In such structure, the IWM is normally supported by additional spring and damper from unsprung mass, so that the IWM is flexibly connected to the sprung mass and unsprung mass [9]. Based on the above-mentioned vibration-absorbing structure, Meng et al. designed a new electric wheel structure with a two-stage internal suspension which can simultaneously transmit energy and isolate system vibrations [10]. Nevertheless, suspended IWM are basically different types of passive vibration isolators. Since the suspension and suspended device parameters are designed under normal operating conditions, it can hardly obtain satisfactory performance under various road conditions.

In addition to structure improvements, many active control methods for the IWM-EV vertical vibration system have been presented to improve the riding comfort and stability. In [11] and [12], an active actuator installing between the IWM and the wheel to eliminate the road roughness affection, which offers a foundation of the active vibration control for IWMs' application. An output feedback H-infinite controller for IWM active suspension system was proposed by Shao et al. to deal with actuator fault while achieving better vertical performance [13]. As the driving motor dynamics will affect the vehicle vertical characteristics, some researchers attempted to consider the influence of motor unbalanced radial force during the IWM design process. The coupling relationship between rotor eccentricity and road excitation and the action mechanism of unbalanced radial force were discussed in [14], which will noticeably diminish the vehicle's response performance. Hu investigated the vibration issues of SRM related to vehicle driving and vibration model, both current chopping controller and active suspension controller were designed to reduce the unbalanced force and improve the vehicle vertical characteristics [15].

However, the above-mentioned literatures mainly focus on suspended device optimization or active control research, and there are few studies that consider the dynamic coupling and integrated control of dynamic vibration absorber and suspension system. To address the above issues and improve the vertical vibration performance of IWM EVs with SRM dynamic, this paper presents an optimization and control study of the IWM-suspension system, which combines both hybrid control strategy and the dynamic vibration absorber to improve vehicle vertical performance. The main contributions of this paper can be summarized as follows:

1) Based on the IWM-suspension system with suspended motor structure, an optimal matching method for the suspension and dynamic vibration absorber parameters is studied to improve the vertical vibration performance.

2) A hybrid control method using the classical skyhook and ground hook control method is utilized for the new IWM-suspension model to further improve the riding comfort and handling stability while reducing the external disturbance effect on the magnetic gap deformation.

The rest of the paper is organized as follows. The IWM-suspension model with SRM and dynamic vibration absorber is explained in Section 2. Cuckoo search based op-

timal matching algorithm is proposed in Section 3. In Section 4, hybrid semi-active controller considering the vibration absorber dynamic is designed. Optimization and control results are validated and discussed in Section 5, and Section 6 concludes the study.

2. System modelling

This section mainly focuses on the modelling of IWM-suspension, including motor model and vehicle suspension model. Firstly, the SRM analytical model with unbalanced radial force is described, and then the vehicle vertical vibration model with SRM dynamic and vibration absorber structure is established.

2.1. Model of switched reluctance motor

Assuming that the electromagnetic parameters and structure of each phase of the switched reluctance motor are symmetrical, the electromotive force balance equation of the first phase of the motor can be written as:

$$u_k = R_k i_k + \frac{d\psi_k}{dt}, \tag{1}$$

where: u_k, i_k and R_k represent the phase winding voltage, current and resistance, respectively; ψ_k is the *k*th phase flux, which can be expressed as a function of winding current and rotor displacement angle:

$$\psi_k = \psi\left(i_1, i_1, ..., i_q; \theta\right), \tag{2}$$

where: *q* is the number of stator phases.

As the mutual inductance between the phases of the switched reluctance motor is much smaller than that of the self-inductance, the *k*th phase flux linkage equation can be obtained by ignoring the mutual inductance between the phases:

$$\psi_k = \psi_k\left(i_k, \theta\right) = \int_0^{i_k} L_k\left(i_k, \theta\right) di_k, \tag{3}$$

among which, $L_k\left(i_k, \theta\right)$ is the stator phase self-inductance represented by the rotor position θ and the winding current i_k. Then Eq. (1) can be expanded into:

$$u_k = RR_k i_k + L_k\left(i_k, \theta\right)\frac{di_k}{dt} + \omega\frac{\partial\psi_k\left(i_k, \theta\right)}{\partial\theta}, \tag{4}$$

where: ω indicates the rotational angular velocity of the rotor. From Eq. (4), the stator winding current can be obtained as follows:

$$i_k = \int \frac{u_k - R_k i_k - \omega\dfrac{\partial\psi_k\left(i_k, \theta\right)}{\partial\theta}}{L_k\left(i_k, \theta\right)} dt. \tag{5}$$

Since the inductance of each phase is periodic, and the harmonic component of the phase inductance is much smaller than the fundamental wave component, the first three terms of the Fourier series can be used to represent the phase self-inductance related to the rotor position [16]:

$$L\left(i, \theta\right) = L_0\left(i\right) + L_1\left(i\right)cos\left(N_r\theta + \varphi_1\right) + \\ + L_2\left(i\right)cos\left(2N_r\theta + \varphi_2\right), \tag{6}$$

where: N_r is the number of rotor poles; φ_n represents the phase angle of the *n*th harmonic and $\varphi_n = n\pi$. $L_0\left(i\right)$, $L_1\left(i\right)$ and $L_2\left(i\right)$ can be expressed as [17]:

$$\begin{bmatrix} L_0\left(i\right) \\ L_1\left(i\right) \\ L_2\left(i\right) \end{bmatrix} = \begin{bmatrix} \frac{1}{4} & \frac{1}{2} & \frac{1}{4} \\ \frac{1}{2} & 0 & -\frac{1}{2} \\ \frac{1}{4} & -\frac{1}{2} & \frac{1}{4} \end{bmatrix} \begin{bmatrix} L_a \\ L_m \\ L_m \end{bmatrix}. \tag{7}$$

Among them, $L_a\left(i\right) = L\left(0, i\right)$ represents the inductance of the pole-aligned position; $L_u\left(i\right) = L\left(\pi/N_r, i\right)$ represents the inductance of the misaligned position, and $L_m\left(i\right) = L\left(\pi/2N_r, i\right)$ represents the inductance of the intermediate position. For there is no saturation at unaligned position, $L_u\left(i\right)$ can be regarded as a constant independent of the current; $L_a\left(i\right)$ and $L_m\left(i\right)$ can be fitted to the following polynomials [18 – 19]:

$$L_a\left(i\right) = \sum_{n=0}^{N} a_n i^n, \quad L_m\left(i\right) = \sum_{n=0}^{N} b_n i^n. \tag{8}$$

By substituting Eqs. (7) and (8) into Eq. (6), the *k*th phase inductance can be obtained as:

$$L_k\left(i_k, \theta\right) = \frac{1}{2}\left[cos^2\left(N_r\theta\right) - cos\left(N_r\theta\right)\right]\sum_{n=0}^{N} a_n i_k^n + \\ + sin^2\left(N_r\theta\right)\sum_{n=0}^{N} b_n i_k^n + \frac{1}{2}\left[cos^2\left(N_r\theta\right) + cos\left(N_r\theta\right)\right]L_u. \tag{9}$$

Incorporating Eq. (9) into Eq. (3), the phase flux linkage equation can be got:

$$\psi_k\left(i_k, \theta\right) = \frac{1}{2}\left[cos^2\left(N_r\theta\right) - cos\left(N_r\theta\right)\right]\sum_{n=0}^{N}\frac{a_{n-1}}{n} i_k^n + sin^2\left(N_r\theta\right)\sum_{n=0}^{N}\frac{b_{n-1}}{n} i_k^n + \frac{1}{2}\left[cos^2\left(N_r\theta\right) + cos\left(N_r\theta\right)\right]L_u i_k. \tag{10}$$

The mechanical energy of the single-phase output of the SRM can be expressed as:

$$W_m = \int_0^i \psi\left(\theta, i\right) \mathrm{d}i. \tag{11}$$

According to the electromechanical energy conversion, the generalized electromagnetic force F_k can be obtained as:

$$F_k = \left.\frac{\partial W_m}{\partial x}\right|_{i = const} = \int_0^i \frac{\partial\psi\left(\theta, i\right)}{\partial x} di. \tag{12}$$

For a four-phase (8/6) pole switched reluctance motor, the total output generalized force is:

$$F = \sum_{k=1}^{4} F_k , \tag{13}$$

where: $k = 1,2,3,4$ represent the force of different phases; x is the generalized displacement and can represent the rotor position angular displacement θ; the air gap between the stator and the rotor l_g; the stator iron stack thickness l_z, which correspond to the electromagnetic driving force, radial electromagnetic force and axial force of the motor, respectively. The axial force has little effect on vehicle dynamics and generally not considered, the electromagnetic drive torque and radial electromagnetic force of the motor can be written as:

$$\begin{aligned} T_e &= \left.\frac{\partial W_m}{\partial \theta}\right|_{i=const} = \int_0^i \frac{\partial \psi(\theta,i)}{\partial \theta} di \\ F_r &= \left.\frac{\partial W_m}{\partial l_g}\right|_{i=const} = \int_0^i \frac{\partial \psi(\theta,i)}{\partial l_g} di \end{aligned} . \tag{14}$$

It can be seen from Eq. (10) that ignoring the term with the denominator i_k, the simplified partial differential equation of the kth phase flux linkage to the rotor position angular displacement θ can be given as:

$$\begin{aligned} \frac{\partial \psi_k(i_k,\theta)}{\partial \theta} &= sin(N_r\theta)\sum_{n=0}^{N} c_n i_k^n + \\ &+ sin(2N_r\theta)\sum_{n=0}^{N} d_n i_k^n , \end{aligned} \tag{15}$$

where: $d_1 = \frac{1}{2}N_r(2b_0 - a_0 - L_u)$; $c_n = \frac{1}{2}N_r\frac{a_{n-1}}{n}$; $c_0 = 0$; $d_0 = 0$; $c_1 = \frac{1}{2}N_r(a_0 - L_u)$; $d_n = N_r\frac{b_{n-1}}{n} - \frac{1}{2}N_r\frac{a_{n-1}}{n}$.

By incorporating Eq. (15) into the electromagnetic drive torque Eq. (14), the motor output torque can be obtained:

$$\begin{aligned} T_e &= \\ &= \sum_{k=1}^{4}\left(sin(N_r\theta)\sum_{n=1}^{N}\frac{1}{n}c_{n-1}i_k^n + sin(2N_r\theta)\sum_{n=1}^{N}\frac{1}{n}d_{n-1}i_k^n \right). \end{aligned} \tag{16}$$

Assuming that the vertical absolute displacement of the air gap between the stator and the rotor is ε, ignoring the salient pole edge magnetic flux, the kth phase winding unbalanced radial electromagnetic force of the SRM is as:

$$F_{rk} = \frac{T_k\delta}{l_g + \varepsilon\cos\beta_k} - \frac{T_k\delta}{l_g - \varepsilon\cos\beta_k} . \tag{17}$$

In the above equation, δ is the coincidence angle of the salient poles of the stator and rotor; β_k is the angle between the axis of the poles and the y-axis when the salient poles of the stator and rotor are coincident. For a four-phase switched reluctance motor, this angle can be expressed as $\beta_k = (k-1)\pi/2, k = 1,2,3,4$. Then the vertical component of the unbalanced radial force is:

$$F_{rkZ} = \sum_{k=1}^{4} F_{rk}\cos\beta_k . \tag{18}$$

2.2. Motor-suspension model

Traditional IWM-suspension model regards the stator and the rotor as a bearing connection when considering the motor electromagnetic force, as shown in 0a, and the dynamic model is as follows:

$$\begin{aligned} &m_b\ddot{x}_b + k_s(x_b - x_{sa}) + c_s(\dot{x}_b - \dot{x}_{sa}) = 0 \\ &m_{sa}\ddot{x}_{sa} + k_{sa}(x_{sa} - x_{wa}) + F_d - k_s(x_b - x_{sa}) - c_s(\dot{x}_b - \dot{x}_{sa}) = 0 \\ &m_{wa}\ddot{x}_{wa} + k_t(x_{wa} - x_z) - k_{sa}(x_{sa} - x_{wa}) - F_d = 0 \end{aligned} . \tag{19}$$

where: m_b is the sprung mass; m_{sa} is the mass of the stator and axle assembly; m_{wa} is the total mass of the rotor and the tire; k_s, c_s and k_{sa} are the suspension stiffness, damping and bearing stiffness, respectively. The stator and rotor displacements are x_{sa} and k_{wa} respectively; k_t represents the tire stiffness; x_b is the sprung mass vertical displacement; x_z denotes the road roughness input. The unbalanced radial force is termed as F_d.

Considering that the wheel hub drive motor is generally placed inside the wheel, the structure of the vibration isolation element between the stator and the body is more complicated and easier to interfere with the original suspension, a vibration absorber with spring and damper can be arranged between motor stator and vehicle axle to improve the space arrangement efficiency and form the wheel dynamic vibration absorber configuration by converting the motor mass into the suspended mass in the wheel space, as shown in 0b. The IWM-suspension model with dynamic vibration absorber structure can be written as:

$$\begin{aligned} &m_b\ddot{x}_b + k_s(x_b - x_{k1}) + c_s(\dot{x}_b - \dot{x}_{k1}) = 0 \\ &m_r\ddot{x}_r + k_b(x_r - x_s) + F_d = 0 \\ &m_s\ddot{x}_s + k_d(x_s - x_{k1}) + c_d(\dot{x}_s - \dot{x}_{k1}) - k_b(x_r - x_s) - F_d = 0 \\ &m_{k1}\ddot{x}_{k1} + k_{sa}(x_{k1} - x_{w1}) - k_s(x_b - x_{k1}) - c_s(\dot{x}_b - \dot{x}_{k1}) - k_d(x_s - x_{k1}) - c_d(\dot{x}_s - \dot{x}_{k1}) = 0 \\ &m_{w1}\ddot{x}_{w1} + k_t(x_{w1} - x_z) - k_{sa}(x_{k1} - x_{w1}) = 0 \end{aligned} , \tag{20}$$

among which, m_{k1}, m_r and m_s represent the axle mass, rotor mass and stator mass, respectively. k_d and c_d are the dynamic vibration absorber parameters; m_{w1} is the assembly mass of tire and rim; x_r and x_s are the rotor and stator vertical displacement, respectively.

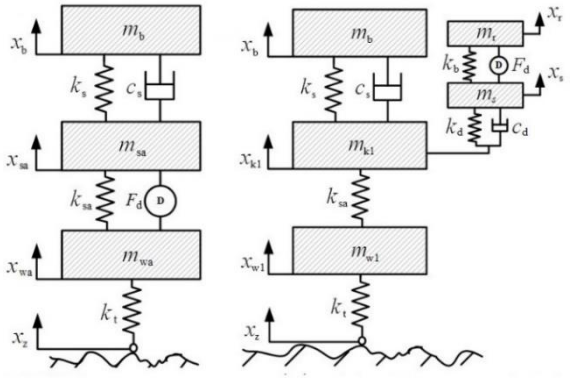

a b

Fig. 1 IWM-suspension model: a) traditional IWM-suspension model; b) IWM-suspension model with dynamic vibration absorber

3. Optimal matching between the suspension and dynamic vibration absorber

3.1. Problem statements

The main role of vehicle vertical dynamic system is to improve the riding comfort and maintain stability. The sprung mass acceleration and tire deflection are always selected as the performance evaluation indices. For the motor dynamic model, the unbalance radial force is closely related to the magnetic gap change, which is arise from road roughness. Therefore, to achieve better performance while making the best optimal matching between the suspension and dynamic vibration absorber, the magnetic gap deflection is also chosen as the optimization index. Based on the above analyses, the optimal object function under single road excitation can be written as:

$$\min_{X\in\Delta} J_{\Omega}(X)=\left[f_{acc}(X), f_{td}(X), f_{mgd}(X)\right], \tag{21}$$

where: X represents the optimization variables including suspension and dynamic vibration absorber parameters; $J_{\Omega}(X)$ is the fitness function in working area Ω; $f_{acc}(X)$, $f_{td}(X)$ and $f_{mgd}(X)$ are the root mean square (RMS) value of sprung mass acceleration, tire deflection and magnetic gap deflection, respectively.

Although the optimal matching can obtain better parameters for the vibration isolation system, the optimization processes are always performed on single road excitation. Therefore, the balance performance under different road excitations should be considered comprehensively. To cover the natural frequencies of sprung and unsprung masses while meeting the actual driving conditions, the vehicle speed is selected as 60 km/h. Considering the real-world road roughness type, B, C and D-level roads are chosen as the external input, and the optimal matching is implemented under three typical road excitations. Vehicle total driving time is 30 seconds, and it travels for 10 seconds on the B, C and D-level roads respectively.

Then the optimal object function under multiple road roughness input can be given as:

$$\min_{X\in\Delta} S_{\Omega}(X)=\left[J_B(X), J_C(X), J_D(X)\right], \tag{22}$$

where: $S_{\Omega}(X)$ is the fitness value under various road excitations; $J_B(X)$, $J_C(X)$ and $J_D(X)$ are the objective values of Eq. (21) with *B*, *C* and *D*-level roads input. In this study, the multiple road excitation case is transformed to a single objective problem through assigning weighting coefficients, which can be expressed as:

$$\min_{X\in\Delta} S_{\Omega}(X)=\lambda_1 J_B(X)+\lambda_2 J_C(X)+\lambda_3 J_D(X). \tag{23}$$

By applying the same method, Eq. (21) can be rewritten as:

$$\min_{X\in\Delta} J_{\Omega}(X)=w_1 f_{acc}(X)+w_2 f_{td}(X)+w_3 f_{mgd}(X), \tag{24}$$

where: λ_i and $w_i\ (i=1,2,3)$ are the weighting coefficients, $\lambda_1+\lambda_2+\lambda_3=1$, $w_1+w_2+w_3=1$. $J_B(X)$, $J_C(X)$ and $J_D(X)$ are the objective values of (24) with three different road profiles, respectively.

The traditional suspension and new dynamic vibration absorber mechanism parameters are chosen as optimal variables, including the stiffness and damping coefficients. To reduce the probability of the suspension hitting the limit block, the specific value of standard deviation $\sigma(f_{sd})$of the suspension deflection to the maximum stroke f_{sd} should satisfy $\sigma(f_{sd})/|f_{sd}|\le 1/3$.

3.2. Cuckoo search (CS) based optimization algorithm

Cuckoo search algorithm is a global search method proposed by Yang et al. in 2009 to simulate the behavior of cuckoo searching for nests and laying eggs [20]. CS is a new search algorithm based on population iteration, which has the advantages of easy implementation and fewer parameter setting, and it has been proved to genetic algorithm and particle swarm optimization algorithm in term of convergence speed and stability [21].

The cuckoo's special habit is parasitic brooding, which means that it has a certain probability of changing the nest, and the probability can be represented by P_a. The flight path of the cuckoo in the process of finding its nest shows the characteristic of Lévy flight, which is a kind of random walk. Through combining the local and global random walking strategy, CS can expand the search range, increase the diversity of the population, and make it easier to jump out of the local optimal solution. The local random walking can be given as:

$$X_i^{t+1}=X_i^t+\gamma H(p_a-\varepsilon)\otimes\left(X_j^t-X_k^t\right), \tag{25}$$

where: $\gamma,\varepsilon\in[0,1]$ and obey uniform distribution. X_i^t, X_j^t and X_k^t are three random individuals in the *t*th generation. $H(p_a-\varepsilon)$ is the Heaviside function, and $\otimes$ represents the pointwise multiplication.

The Lévy flight based global random walking characteristic can be written as:

$$X_i^{t+1} = X_i^t + \alpha L(\lambda), \tag{26}$$

where: X_i^{t+1} is the individual i in the tth generation; α is the step size control parameter which is used to control the search range. Lévy random number $L(\lambda)$ can be expressed as:

$$L(s,\beta) = \phi \times u / |v|^{1/\beta}, \tag{27}$$

where: u and v obey standard normal distribution, the value range of β is $[1,2]$, and the value of ϕ is as follows:

$$\phi = \left\{ \frac{\Gamma(1+\beta)\sin(\pi\beta/2)}{\Gamma\left[(1+\beta)/2\right]\beta \times 2^{(\beta-1)/2}} \right\}^{1/\beta}, \tag{28}$$

among which Γ is the Gamma distribution, and $\Gamma = \int_0^\infty e^{-t} t^{\lambda-1} dt$.

3.3. Parameter optimization

The cuckoo search algorithm is employed to acquire the optimal solutions of the suspension and dynamic vibration absorber. The number of cuckoo nests is chosen as 200, and the iterations are 100. The single road excitation objective function weighting parameters w_1=0.5, w_2=0.3, and w_3=0.2, among which the riding comfort is the main optimization object on the basis of handling stability. The multiple road excitation objective function weighting parameters λ_1, λ_2 and λ_3 are all 1/3, which means that the optimization goals are the same with three different road inputs. The evolution process of the CS algorithm is plotted in 0, and it can be seen from the figure that the search process converges to the final fitness value within 20 generations.

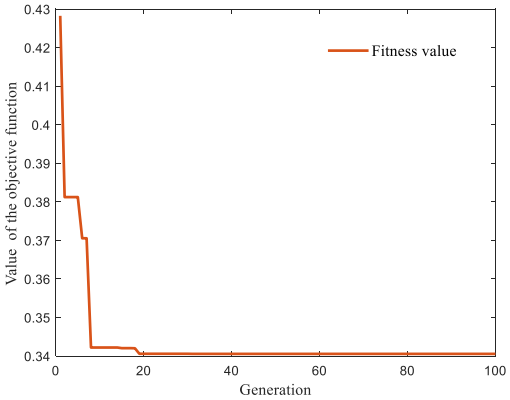

Fig. 2 Evolution process of the cuckoo search algorithm

4. Hybrid semi-active controller design

4.1. Basic theory of skyhook

Similar to the traditional suspension system, the EV suspension with IWM dynamic has the property that the riding comfort and handling stability can hardly be optimized simultaneously. This is because the passive spring and damper installed between the vehicle body mass and the wheel mass will have opposite effects on the sprung and unsprung masses. If one end of the shock absorber is fixed to the inertial reference system instead of fixed between the two masses, the damping force will not act on the two masses simultaneously. With respect to the position of the inertial reference system, such control methods are divided into skyhook control and groundhook control [22].

The concept of skyhook damping control was first proposed by Karnopp [23], and the structure effectively reduces the sprung mass vibration by installing a shock absorber between the vehicle's sprung mass and the inertial reference. Considering that the shock absorber installed between the sprung mass and the inertial reference cannot be realized in practical applications, it can be converted to obtain an equivalent skyhook damping system. A modified skyhook controller with passive damping coefficient $C_{p\text{-}sky}$ are proposed to deal with the unwanted harshness [24], as shown in 0.

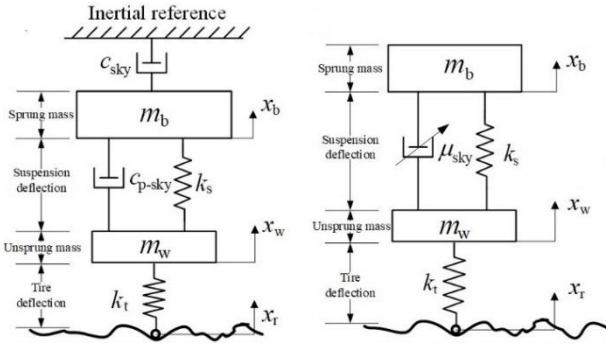

a b

Fig. 3 Skyhook damping control structure: a) modified skyhook model; b) equivalent modified skyhook model

Through comparing the dynamic equations of the modified skyhook model and equivalent modified model, to make the modified skyhook model to achieve equivalent performance to that of the ideal skyhook control, the following equations need to be satisfied:

$$\mu_{sky} = c_{p\text{-}sky} + \frac{c_{sky}\dot{x}_b}{(\dot{x}_b - \dot{x}_w)}. \tag{29}$$

Then, the modified skyhook control force can be expressed as:

$$F_d = \begin{cases} c_{p\text{-}sky}(\dot{x}_b - \dot{x}_w) + c_{sky}(\dot{x}_b), & if\ (\dot{x}_b - \dot{x}_w)\cdot\dot{x}_b > 0 \\ c_{min}(\dot{x}_b - \dot{x}_w), & if\ (\dot{x}_b - \dot{x}_w)\cdot\dot{x}_b < 0 \end{cases}. \tag{30}$$

Meanwhile, to ensure that the maximum output of the equivalent skyhook damping control force satisfies the limit working conditions and energy dissipation constraints of the shock absorber, the equivalent skyhook damping control force should satisfy the following equations:

$$F_d^{output} = \begin{cases} F_d^{max}, & if\ F_d > F_d^{max} \\ F_d, & if\ F_d^{max} > F_d > F_d^{min} \\ F_d^{min}, & if\ F_d^{min} > F_d \end{cases}. \tag{31}$$

where: F_d^{max} and F_d^{min} are the upper and lower limit forces of the damper, respectively.

Similar to the skyhook control, the groundhook can dampen the wheel vertical vibration by installing a shock absorber between the unsprung mass and the inertial reference, so as to achieve the purpose of improving the handling stability. The control law of the groundhook control can be given as:

$$F_{grd} = \begin{cases} c_{grd}\left(\dot{x}_w\right), & if\ -\left(\dot{x}_b - \dot{x}_w\right)\times \dot{x}_w\, 30 \\ c_{min}\left(\dot{x}_b - \dot{x}_w\right), & if\ -\left(\dot{x}_b - \dot{x}_w\right)\times \dot{x}_w < 0 \end{cases}. \tag{32}$$

4.2. Hybrid control of the IWM-suspension system

The skyhook control takes the sprung mass state as the controller input to suppress the sprung mass acceleration, and the groundhook control takes the unsprung mass state as the input to inhibit the tire bounce. Therefore, to achieve the purpose of improving riding comfort and handling stability simultaneously, it is necessary to combine the merits of both control method, which is the hybrid control.

In view to the special structure of the IWM-suspension system, the purpose of the designed model is to reduce the road roughness and motor vibration impact on the sprung mass motion while keeping the tire in constant contact with the road surface. Besides, the gap between the stator and rotor also needs to be followed for that the magnetic gap is the direct cause of electromagnetic disturbance force which has an important impact on the working environment of the motor. Therefore, the motor dynamic should be considered in the controller design process. As shown in 0a, the hybrid controller with two virtual skyhook dampers are put forward for the IWM-suspension model, and the equivalent hybrid control model is given in 0b.

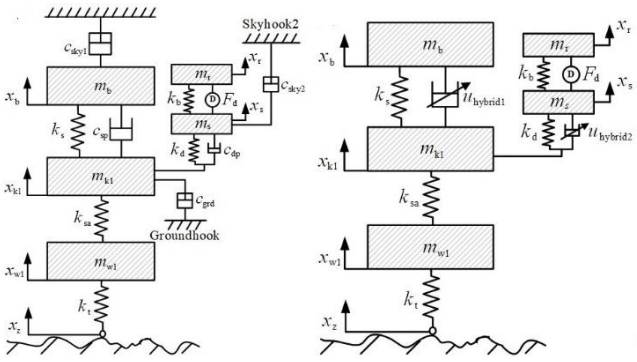

Fig. 4 Suspension-motor vertical vibration control model: a) ideal hybrid control model; b) equivalent hybrid control model

The dynamic equations of the ideal hybrid control dynamic equations are listed as follows:

$$\begin{aligned}
&m_b\ddot{x}_b + k_s\left(x_b - x_{k1}\right) + c_{sp}\left(\dot{x}_b - \dot{x}_{k1}\right) + c_{sky1}\dot{x}_b - c_{grd}\dot{x}_{k1} = 0 \\
&m_r\ddot{x}_r + k_b\left(x_r - x_s\right) + F_d = 0 \\
&m_s\ddot{x}_s + k_d\left(x_s - x_{k1}\right) + c_{dp}\left(\dot{x}_s - \dot{x}_{k1}\right) + c_{sky2}\dot{x}_s + c_{grd}\dot{x}_{k1} - k_b\left(x_r - x_s\right) - F_d = 0 \\
&m_{k1}\ddot{x}_{k1} + k_{sa}\left(x_{k1} - x_{w1}\right) - k_s\left(x_b - x_{k1}\right) - c_{sp}\left(\dot{x}_b - \dot{x}_{k1}\right) - k_d\left(x_s - x_{k1}\right) - c_{dp}\left(\dot{x}_s - \dot{x}_{k1}\right) - c_{sky2}\dot{x}_s - c_{grd}\dot{x}_{k1} = 0 \\
&m_{w1}\ddot{x}_{w1} + k_t\left(x_{w1} - x_z\right) - k_{sa}\left(x_{k1} - x_{w1}\right) = 0
\end{aligned} \tag{33}$$

Since the controllable dampers are mounted in the place of c_{sp} and c_{dp}, both the sprung mass m_b and stator mass m_s are influenced by the groundhook coefficient c_{grd}. Then the equivalent hybrid control equation can be given as:

$$\begin{aligned}
&m_b\ddot{x}_b + k_s\left(x_b - x_{k1}\right) + m_{hybrid1}\left(\dot{x}_b - \dot{x}_{k1}\right) = 0 \\
&m_r\ddot{x}_r + k_b\left(x_r - x_s\right) + F_d = 0 \\
&m_s\ddot{x}_s + k_d\left(x_s - x_{k1}\right) + m_{hybrid2}\left(\dot{x}_s - \dot{x}_{k1}\right) - k_b\left(x_r - x_s\right) - F_d = 0 \\
&m_{k1}\ddot{x}_{k1} + k_{sa}\left(x_{k1} - x_{w1}\right) - k_s\left(x_b - x_{k1}\right) - c_s\left(\dot{x}_b - \dot{x}_{k1}\right) - k_d\left(x_s - x_{k1}\right) - m_{hybrid2}\left(\dot{x}_s - \dot{x}_{k1}\right) = 0 \\
&m_{w1}\ddot{x}_{w1} + k_t\left(x_{w1} - x_z\right) - k_{sa}\left(x_{k1} - x_{w1}\right) = 0
\end{aligned} \tag{34}$$

Through comparing the dynamic Eqs. of (33) and (34), the hybrid coefficients of suspension damper and dynamic vibration absorber damper are as follows:

$$\begin{aligned}
\mu_{hybrid1} &= \frac{c_{sp}\left(\dot{x}_b - \dot{x}_{k1}\right) + c_{sky1}\dot{x}_b - c_{grd}\dot{x}_{k1}}{\dot{x}_b - \dot{x}_{k1}} \\
m_{hybrid2} &= \frac{c_{dp}\left(\dot{x}_s - \dot{x}_{k1}\right) + c_{sky2}\dot{x}_s + c_{grd}\dot{x}_{k1}}{\dot{x}_s - \dot{x}_{k1}}
\end{aligned}. \tag{35}$$

For the hybrid control of IWM-suspension system, the choice of the damping coefficient for one of the control targets will definitely affect the other control target, which complicates the choice of damping parameters. In the actual control, the hybrid system is controlled by changing the value of hybrid coefficients. Therefore, the selection of skyhook and groundhook coefficients will inevitably influence the control effect of the control strategy. And the optimization of aforementioned coefficients of the IWM-suspension can be described as a multi-parameter optimization problem with the goal of improving the ride comfort and handling stability while the suspension deflection and magnetic gap deflection as the constraint. The multi-parameter optimization problem can be expressed as:

$$\begin{aligned}
min: \quad & f_1(P) = rms\left(\ddot{x}_b\right) \\
& f_2(P) = rms\left(x_{w1} - x_z\right) \\
subject\ to: \quad & 3rms\left(x_b - x_{k1}\right) \le lim\left(x_b - x_{k1}\right) \\
& 3rms\left(x_r - x_s\right) \le lim\left(x_r - x_s\right)
\end{aligned}, \tag{36}$$

where: $rms(\ddot{x}_b)$ and $rms(x_{w1}-x_z)$ are the root mean square value of the sprung mass acceleration and tire deflection, $lim(x_b-x_{k1})$ and $lim(x_r-x_s)$ represent the limit deflection of suspension and IWM magnetic gap, respectively. By utilizing the multi-object optimization method described in [22], the control coefficients with optimized riding comfort and handling stability can be obtained, and the pareto front of the riding comfort and handling stability is plotted in 0.

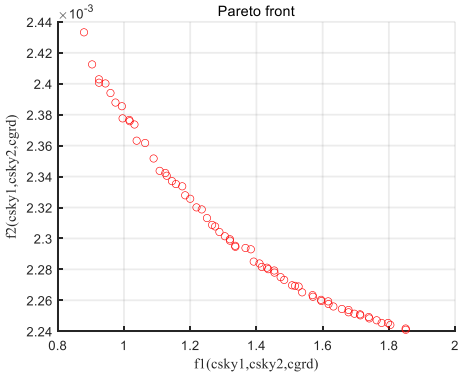

Fig. 5 Pareto optimal solution set

5. Simulation and discussions

In this section, the optimal matching results between the suspension and dynamic vibration absorber parameters are firstly discussed, and the control properties for the IWM-suspension system are presented to illustrate the effectiveness of the hybrid controller. Four performance indexes are discussed, including vehicle sprung mass acceleration (SBA), suspension deflection (SD), tire deflection (TD), and magnetic gap deformation (MGD). The IWM-suspension parameters are listed in 0.

Table 1

IWM-suspension parameters

Traditional suspension parameters	Value	IWM-suspension parameters	Value
m_b	350 kg	m_r	25 kg
k_s	24000 N/m	k_b	7×10⁶ N/m
c_s	2200 Ns/m	m_s	20 kg
m_{sa}	30 kg	k_d	50000 N/m
k_{sa}	7×10⁶ N/m	c_d	2000 N/m
m_{wa}	40 kg	m_{k1}	10 kg
k_t	220000 N/m	m_{w1}	15 kg

5.1. Optimal matching verification

The characteristics of the IWM-suspension system with and without dynamic vibration absorber (DVA) are evaluated by the system indexes, and the root mean square (RMS) values of the two models are listed in 0. The simulation is performed on C-level road with the speed of 60 km/h. From the table, it can be found that the SMA, TD, and SD of the IWM-suspension with DVA structure are all improved compared with the traditional model, where the SMA and TD are reduced by 22% and 17%, respectively. Especially for the IWM dynamic response under the random road profile in terms of MGD, the IWM-suspension with DVA can obtain better performance than the traditional structure with improvements of 70% on average.

Based on the DVA configuration, the optimal matching between the suspension and DVA parameters is carried out, and the optimization parameters before and after optimization are analyzed to verify the feasibility of the designed optimal matching method, and the optimized parameters are given in 0.

Table 2

RMS comparison of tradition and DVA structure

Evaluation index	RMS Value	
	Traditional	With DVA
SMA	1.4967	1.1740
TD	0.0039	0.0032
MGD	9.1269e-05	2.5363e-05
SD	0.0085	0.0082

Table 3

Optimization results

Parameters	Value	
	Before optimization	After optimization
k_s	24000 N/m	23192 N/m
c_s	2200 Ns/m	1680 Ns/m
k_d	50000 N/m	43179 N/m
c_d	2000 Ns/m	1440 Ns/m

To illustrate the optimization effect, the time domain response comparisons for three typical road excitations before and after optimization are plotted in 0a-d. It can be obviously observed that the system responses increase with the road grade. With the optimized parameters, it can be seen from 0a that the SMAs after optimization are reduced in comparison with before optimization, which demonstrates that the vertical vibration performance is improved after optimal matching. The SDs in 0b has increased after optimization, but the constraints are guaranteed under different road excitations. The TDs in 0c is reduced after optimization, which means the handling stability has been improved. Besides, it can be observed from 0d that the MGDs with optimized parameters are much smaller than those with original parameters, indicating the effectiveness of the proposed optimal method under various road surfaces. The RMS comparison of IWM-suspension responses with three typical road level inputs is listed in 0. It is clear that the optimized suspension and DVA parameters can achieve better vertical vibration performance than the unoptimized model.

5.2. Hybrid control validation for the IWM-suspension system

In this section, the C-level road with the speed of 60 km/h is utilized to illustrate the effectiveness of the designed hybrid controller. The time domain responses of the IWM-suspension model are plotted in 0. The SMA with the hybrid controller in 0a has a signification reduction compared to the passive system, demonstrating that the hybrid controller can improve the vehicle riding comfort effectively. Both SD and TD of hybrid controller shown in 0b-c are reduced compared to that of the passive model, which guarantees the suspension constrain while maintain-ing the road-holding stability. The MGD plotted in 0d indicate that with the hybrid controller, the motor dynamic and lifespan can effectively be improved. The detailed RMS value of the controlled and uncontrolled responses are listed in 0.

To further illustrate the capability of the hybrid controller, the frequency domain of the IWM-suspension.

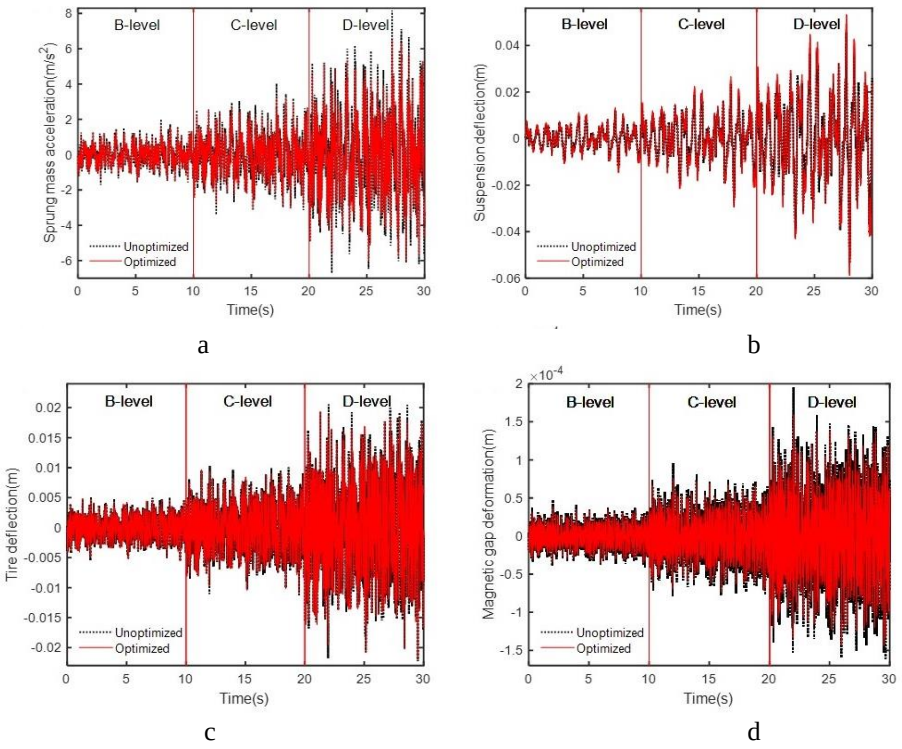

Fig. 6 Dynamic response comparisons of IWM-suspension system before and after optimization: a) sprung mass acceleration; b) suspension deflection; c) tire deflection; d) magnetic gap deformation

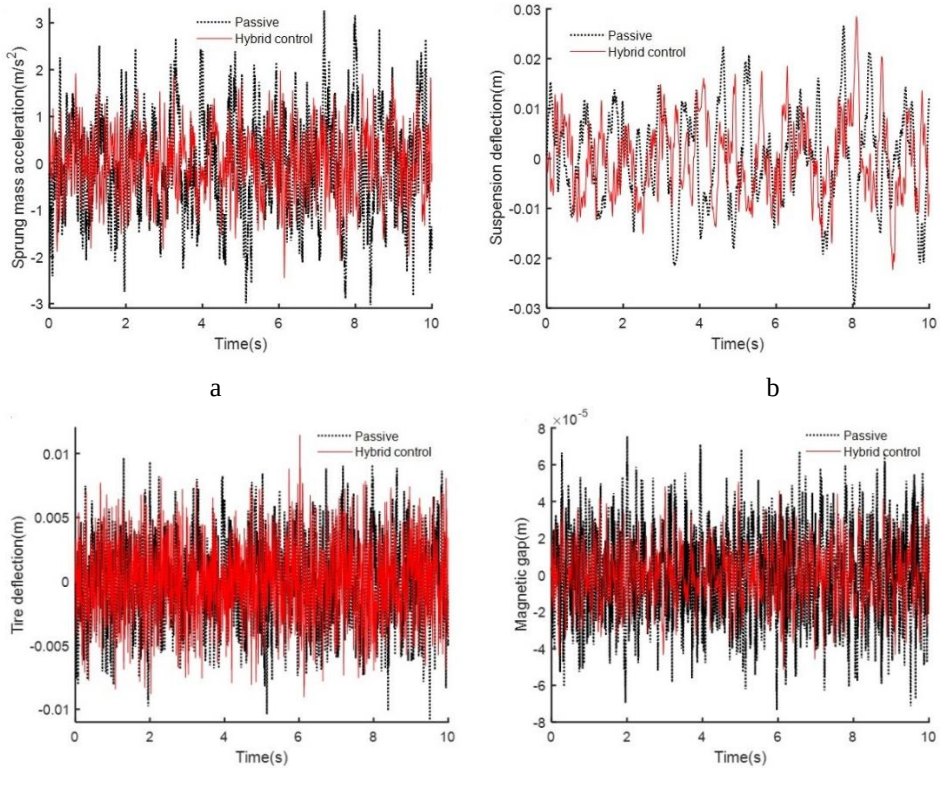

Fig. 7 IWM-suspension dynamic response comparisons with stochastic road: a) sprung mass acceleration; b) suspension deflection; c) tire deflection; d) magnetic gap deformation

Table 4

Index	RMS value of the performance indexes					
	B-level		C-level		D-level	
	Before optimization	After optimization	Before optimization	After optimization	Before optimization	After optimization
SMA	0.587	0.5323	1.1740	1.0646	2.3985	2.1293
TD	0.0016	0.0015	0.0032	0.0031	0.0065	0.0061
MGD	1.2648e-05	1.0993e-05	2.5363e-05	2.2082e-05	5.0905e-05	4.4088e-05
SD	0.0041	0.0047	0.0082	0.0093	0.0164	0.0187

Table 5

Controlled and uncontrolled responses

Index	RMS Value of the time domain responses		
	Passive	Hybrid	Improvement
SMA	1.0646	0.6942	34.79%
TD	0.0031	0.0029	6.45%
MGD	2.2082e-05	1.6383e-05	25.81%
SD	0.0093	0.0083	10.75%

performance indexes are given in 0. For the SMA of first figure, the hybrid control reduces the amplitude in low frequency range, especially around the natural frequency of the body mass. The frequency response of TD is plotted in the second figure, it can be observed from the figure that the controlled and uncontrolled system display similar characteristic in high frequency range, but the controlled system is much better than the uncontrolled system in the natural frequency of the unsprung mass. The third figure shows that with the hybrid controller, the amplitude of the MGD is reduced compared to the passive one at low and middle frequency ranges, which will reduce the impact of unbalanced radial force on the vertical vibration system. Besides, the above analysis also shows that the system responses of the frequency domain are consistent with that of the time domain, thus verifying the effectiveness of the method.

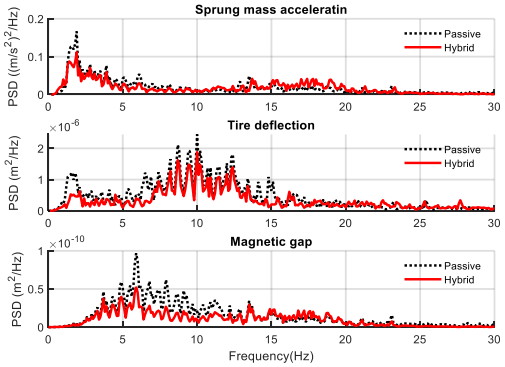

Fig. 8 PSD of IWM-suspension responses

6. Conclusions

This paper presents an optimal and control strategy for IWM-suspension system driven by SRM. Coupled suspension and SRM dynamic model with vibration absorber structure is established, and then the optimal matching and hybrid control are conducted to improve the vertical performance of the system. Finally, numerical simulations are performed under typical road surfaces to demonstrate the effectiveness of the designed method. The following conclusions can be obtained:

1) With the help of optimal matching between suspension and dynamic vibration absorber, the optimized parameters can obviously improve the system performance in term of sprung mass acceleration, tire deflection and magnet gap. 2) According to results from the hybrid control simulation, a 34.79% improvement in riding comfort, 6.45% improvement in handling stability, and 25.81% improvement in magnet gap can be achieved by the proposed control strategy compared to the passive system.

Future work will focus on the integrated control of motor and suspension system to improve the vertical performance under various driving conditions.

Declaration of conflicting interests

The authors declare no conflict of interest.

Acknowledgement

This research was funded by the Natural Science Foundation of Shaanxi Province (No. 2021JQ-857), Shaanxi Provincial Key Research and Development Project (No. 2020ZDLGY16-01), Natural Science Foundation of Shaanxi Province(2022JQ-547) and Scientific Research Plan Projects of Shaanxi Education Department (No. 21JK0700).

References

1. **Qin, Y.; Zhao, Z.; Wang, Z.;** et al. 2021. Study of longitudinal–vertical dynamics for in-wheel motor-driven electric vehicles, Automotive Innovation 4(2): 227-237. https://doi.org/10.1007/s42154-021-00141-5.
2. **Zhao, Z.; Taghavifar, H.; Du, H.;** et al. 2021. In-wheel motor vibration control for distributed-driven electric vehicles: A review, IEEE Transactions on Transportation Electrification 7(4): 2864-2880. https://doi.org/10.1109/TTE.2021.3074970.
3. **Sreejith, R.; Singh, B**. 2020. Sensorless predictive current control of PMSM EV drive using DSOGI-FLL based sliding mode observer, IEEE Transactions on Industrial Electronics 99: 1-1. https://doi.org/10.1109/TIE.2020.2996159.
4. **Zhu, J.; Cheng, K. E.; Xue, X.;** et al. 2017. Design of a novel high-torque-density in-wheel switched reluctance motor for electric vehicles, 2017 IEEE International Magnetics Conference 2017: 1-2. https://doi.org/10.1109/INTMAG.2017.8008065.
5. **Zhou, S.; Walker, P.; Tian, Y.;** et al. 2021. Comparison on energy economy and vibration characteristics of electric and hydraulic in-wheel drive vehicles, Energies 14(8): 2290. https://doi.org/10.3390/en14082290.
6. **Qin, Y.; He, C.; Shao, X.;** et al. 2018. Vibration mitigation for in-wheel switched reluctance motor driven electric vehicle with dynamic vibration absorbing structures, Journal of Sound and Vibration 419: 249-267. https://doi.org/10.1016/j.jsv.2018.01.010.
7. **Wang, Q.; Li, R.; Zhu, Y.;** et al. 2020. Integration design and parameter optimization for a novel in-wheel motor with dynamic vibration absorbers, Journal of the Brazilian Society of Mechanical Sciences and Engineering 42(9): 1-12. https://doi.org/10.1007/s40430-020-02543-8.
8. **Luo, Y.; Tan, D**. 2012. Study on the dynamics of the in-wheel motor system, IEEE Transactions on Vehicular Technology 61(8): 3510-3518. https://doi.org/10.1109/TVT.2012.2207414.
9. **Liu, M.; Zhang, Y.; Huang, J.;** et al. 2020. Optimization control for dynamic vibration absorbers and active suspensions of in-wheel-motor-driven electric vehicles, Proceedings of the Institution of Mechanical Engineers, Part D: Journal of Automobile Engineering 234(9): 2377-2392. https://doi.org/10.1177/0954407020908667.
10. **Meng, L.; Zou, Y.; Qin, Y.;** et al. 2020. A new electric wheel and optimization on its suspension parameters, Proceedings of the Institution of Mechanical Engineers,

Part D: Journal of Automobile Engineering 234(12): 2759-2770.
https://doi.org/10.1177/0954407020921736.
11. **He, R.; Wang, J. C.** 2020. Vertical vibration control of an in-wheel motor-driven electric vehicle using an in-wheel active vibration system, Asian Journal of Control 22(2): 879-896.
https://doi.org/10.1002/asjc.1948.
12. **Ma, Y.; Deng, Z.; Xie, D**. 2013. Control of the active suspension for in-wheel motor, Journal of Advanced Mechanical Design Systems and Manufacturing 7(4): 535-543.
https://doi.org/10.1299/jamdsm.7.535.
13. **Shao, X.; Naghdy, F.; Du, H.;** et al. 2019. Output feedback H∞ control for active suspension of in-wheel motor driven electric vehicle with control faults and input delay, ISA transactions 92: 94-108.
https://doi.org/10.1016/j.isatra.2019.02.016.
14. **Deng, Z.; Li, X.; Liu, T.;** et al. 2021. Modeling and suppression of unbalanced radial force for in-wheel motor driving system, Journal of Vibration and Control 2021: 10775463211026041.
https://doi.org/10.1177/10775463211026041.
15. **Hu, Y.; Li, Y.; Li, Z.;** et al. 2021. Analysis and suppression of in-wheel motor electromagnetic excitation of IWM-EV, Proceedings of the Institution of Mechanical Engineers, Part D: Journal of Automobile Engineering 235(6): 1552-1572.
https://doi.org/10.1177/0954407020979096.
16. **Mahdavi, J.; Suresh G.; Fahimi, B.;** et al. 1997. Dynamic modeling of nonlinear SRM drive with spice, Conference Record of the 1997 IEEE Industry Applications Conference Thirty-Second IAS Annual Meeting 1: 661-667.
https://doi.org/10.1109/IAS.1997.643140.
17. **Fahimi, B.; Suresh, G.; Mahdavi, J.;** et al. 1998. A new approach to model switched reluctance motor drive application to dynamic performance prediction, control and design, 29th Annual IEEE Power Electronics Specialists Conference 2: 2097-2102.
https://doi.org/10.1109/PESC.1998.703469.
18. **Ye, Z. Z.; Martin, T. W.; Balda, J. C.** 2000. Modeling and nonlinear control of a switched reluctance motor to minimize torque ripple, IEEE International Conference on Systems, Man and Cybernetics 5: 3471-3478.
https://doi.org/10.1109/ICSMC.2000.886546.
19. **Krishnamurthy, M.; Edrington, C. S.; Emadi, A.;** et al. 2006. Making the case for applications of switched reluctance motor technology in automotive products, IEEE Transactions on Power Electronics 21(3): 659-675.
https://doi.org/10.1109/TPEL.2006.872371.
20. **Yang, X. S.; Deb, S.** 2013. Multi-objective cuckoo search for design optimization, Computers & Operations Research 40(6):1616-1624.
https://doi.org/10.1016/j.cor.2011.09.026.
21. **Yang, X. S.; Deb, S.** 2009. Cuckoo Search via Lévy flights, World Congress on Nature & Biologically Inspired Computing 2009: 210-214.
https://doi.org/10.1109/NABIC.2009.5393690.
22. **Qin, Y.; Dong, M.; Reza, L.;** et al. 2015. Adaptive hybrid control of vehicle semi-active suspension based on road profile estimation, Shock and Vibration 2015: 1-13.
https://doi.org/10.1155/2015/636739.
23. **Karnopp, D. C.; Crosby, M. J.; Harwood, R. A.** 1974. Vibration control using semi-active force generators, Journal of Engineering for Industry 96(2): 619–626.
https://doi.org/10.1115/1.3438373.
24. **Abu Bakar, S. A.; Jamaluddin, H.; Rahman, R. A.;** et al. 2008. Vehicle ride performance with semi-active suspension system using modified skyhook algorithm and current generator model, International Journal of Vehicle Autonomous Systems 6(3-4): 197-221.
https://doi.org/10.1504/IJVAS.2008.023577.

Jinwei Sun, Jingyu Cong

OPTIMIZATION AND CONTROL OF ELECTRIC VEHICLE VERTICAL SYSTEM WITH SUSPENEDED IN-WHEEL MOTOR

S u m m a r y

This paper presents an optimization and control approach for vehicle vibration system with suspended in-wheel motor to reduce the vertical negative effects. Vibrations caused by the motor unbalanced radial force arising from road surface can be mitigated through the proposed approach. A four quarter in-wheel motor suspension system with dynamic vibration absorber is established, and analytical switch reluctance motor (SRM) model is derived using Fourier series. Cuckoo search based optimal matching method between suspension and vibration isolator parameters is designed to improve the vibration performance while reducing the external disturbance effect on the motor air gap with typical road excitations. On the basis of the optimal matching results, a hybrid control strategy is proposed for the in-wheel motor suspension, and the suspension and isolator dampers are considered as the semi-active device to assign the hybrid control force according to model responses. Simulation results indicate that the optimized model can achieve better vibration characteristics, and the hybrid controller can improve the riding comfort and handling stability effectively.

Keywords: in-wheel motor, vibration control, optimization, dynamic vibration absorber.

Received February 21, 2022
Accepted April 08, 2022